Impact of Detailed Multicomponent Transport on Planar and Counterflow Hydrogen/Air and Methane/Air Flames

Alexandre Ern[a,b,⋆] and Vincent Giovangigli[b]

[a] CERMICS-ENPC, 6 et 8 av. Blaise Pascal, 77455 Marne-la-Vallée cedex 2, France
⋆ ern@cermics.enpc.fr

[b] CMAP-CNRS, Ecole Polytechnique, 91128 Palaiseau cedex, France

Abstract. Freely propagating and counterflow laminar premixed steady hydrogen/air and methane/air flames are investigated numerically using complex chemistry and detailed transport models. All the transport coefficients in the mixture, including thermal diffusion coefficients, are evaluated using cost-effective, accurate algorithms derived recently by the authors from the kinetic theory of gases. Our numerical results provide a quantitative assessment of the impact of thermal diffusion on planar flame speed as a function of equivalence ratio and on extinction limits of counterflow flames as a function of either strain rate or equivalence ratio. In some cases, such as rich hydrogen/air flames, the effect of thermal diffusion is actually opposite to the one expected from a qualitative viewpoint or obtained with empirical models. In addition, we observe relevant effects of thermal diffusion on extinction of methane/air counterflow flames.

Keywords. Multicomponent transport, thermal diffusion, freely propagating flames, counterflow flames.

1 INTRODUCTION

Freely propagating and counterflow laminar premixed flames are on the natural route to recent theories of multidimensional turbulent flames, predictions of chemically controlled extinction limits and further understanding of pollutant formation in combustion applications. As a result, extensive interest has been devoted over the last decade to

both experimental and computational models of such flames. Ideally, numerical models would combine complex chemical kinetics with detailed multicomponent transport models in order to predict accurately flame structure, planar flame speed and flame extinction in function of various operating parameters. However, while detailed chemical reaction mechanisms for both hydrogen/air and methane/air flames are now routinely used in numerical models, much less attention has been paid to the accuracy of the model for multicomponent transport.

One of the most challenging multicomponent transport phenomena is thermal diffusion because evaluating the corresponding kinetic theory expressions is a formidable computational task. Thermal diffusion is a cross-transport phenomenon which gives rise to the Soret and Dufour effects, the former corresponding to an additional term in the species diffusion velocities proportional to the temperature gradient and the latter to an additional term in the heat flux vector. From a qualitative viewpoint, it is well-known that the Soret effect tends to drive light molecules towards hot regions and heavy molecules towards cold regions of the flow. It is thus expected to be particularly important in the presence of strong temperature gradients such as those found in chemically reacting flows.

The impact of multicomponent transport on one-dimensional flames has been studied first in the pioneering work of Dixon-Lewis (1968). In particular, for hydrogen/air flames, it was observed that the molar diffusion flux and the thermal diffusion flux for hydrogen and nitrogen could be of the same order of magnitude. Greenberg (1980) made the same observation in the study of one-dimensional hydrogen/air flames using a single step chemistry model and phenomenological expressions for the thermal diffusion coefficients. Later, Warnatz (1982) found that the laminar flame speed of hydrogen/air flames was slightly lower when thermal diffusion was taken into account. This result was obtained for both lean and rich flames, but thermal diffusion was modeled using semi-empirical expressions and only for the diffusion flux of atomic and molecular hydrogen. We shall see that for rich flames this result is at variance with the present results where kinetic theory expressions are used for the thermal diffusion coefficients of all the chemical species. Kinetic theory expressions for thermal diffusion coefficients have been considered by Heimerl and Coffee (1982), but the authors only studied a few flames for which detailed multicomponent transport algorithms did not appear to be critical. We shall see that such conclusion is again at variance with the one of the present work. Recent studies sheding new light upon the importance of the Soret effect include the theoretical analysis of the structure of a wrinkled premixed flame (García-Ybarra *et al.*, 1984), and numerical models of hydrogen jet diffusion flames (Hancock *et*

al., 1996), laminar methane flames (Popp and Baum, 1997), chemical vapor deposition reactors (Ern *et al.*, 1996) and hydrogen/air and methane/air bunsen flames (Ern and Giovangigli, 1998).

An important step toward detailed modeling of multicomponent transport has been achieved recently. Indeed, in the framework of the theory derived by the authors (1994, 1995, 1996a, 1996b), it is possible to evaluate at a moderate computational cost all the transport coefficients in gas mixtures using rigourous accurate expressions. As an application of this theory, the present work focuses on freely propagating and counterflow premixed hydrogen/air and methane/air flames. Its contributions are three-fold. First, it provides for the first time a thorough and quantitative assessment of the role played by multicomponent transport in such flames. In addition, our numerical results show that in some cases, such as rich hydrogen/air flames, the effect of thermal diffusion is actually opposite to the one expected from a qualitative viewpoint or obtained with empirical models. Finally, we observe relevant effects of thermal diffusion on the extinction of methane/air counterflow flames.

The paper is organized as follows. In the next section we formulate the governing equations for both freely propagating and counterflow steady laminar flames and briefly discuss the mathematically appropriate boundary conditions. In Section 3 we shortly review the theoretical background for multicomponent transport algorithms. In Section 4 we describe the solution method. In Sections 5 and 6 we present the numerical results obtained for freely propagating and counterflow flames, respectively.

2 PROBLEM FORMULATION

In this section we present the conservation equations and boundary conditions for freely propagating and counterflow laminar premixed steady flames. Considering first freely propagating flames, our goal is to predict the species mass fractions and temperature profiles as a function of the independent spatial coordinate normal to the flame front, along with the mass flow rate which is an eigenvalue of the problem. Let x denote the spatial coordinate, $Y_1, \ldots, Y_n$ the species mass fractions, T the temperature and m the mass flow rate. The governing equations read

$$m d_x Y_i = - d_x(\rho Y_i U_i) + m_i \omega_i, \qquad i \in [1,n], \tag{1}$$

$$m c_p d_x T = - d_x \widetilde{Q} - \Big(\sum_{i \in [1,n]} \rho Y_i U_i c_{pi} \Big) d_x T - \sum_{i \in [1,n]} h_i m_i \omega_i, \tag{2}$$

completed with the ideal gas law

$$\rho = \frac{p\overline{m}}{RT}. \tag{3}$$

Here, we have introduced the spatial derivative operator d_x, the density ρ, the diffusion velocity of the i^{th} species U_i, the molecular weight of the i^{th} species m_i, its molar production rate ω_i, the specific heat capacity at constant pressure of the mixture c_p, the thermal heat flux $\widetilde{Q}$ given by $\widetilde{Q} = Q - \sum_{i\in[1,n]} h_i \rho Y_i U_i$ where Q is the heat flux, the specific heat capacity at constant pressure of the i^{th} species c_{pi}, its specific enthalpy h_i, the pressure p, the mean molecular weight of the mixture $\overline{m}$, and the ideal gas constant R. Since freely propagating flames are in the low Mach number regime, the pressure in the ideal gas law can be taken as constant while the hydrodynamic pressure uncouples from the governing equations (1)–(3) and can be recovered from their solution.

The species diffusion velocities and the thermal heat flux are given from the kinetic theory of gases (Waldmann and Trübenbacher, 1962, Ferziger and Kaper, 1972) as follows

$$U_i = -\sum_{j\in[1,n]} D_{ij}(d_x X_j + X_j \widetilde{\chi}_j d_x \log T), \qquad i \in [1,n], \tag{4}$$

$$\widetilde{Q} = -\lambda d_x T + p \sum_{i\in[1,n]} X_i \widetilde{\chi}_i U_i, \tag{5}$$

where $D = (D_{ij})_{i,j\in[1,n]}$ is the diffusion matrix, X_i the mole fraction of the i^{th} species, $\widetilde{\chi} = (\widetilde{\chi}_i)_{i\in[1,n]}$ the thermal diffusion factors, and λ the thermal conductivity. The thermal diffusion factors satisfy $X_i\widetilde{\chi}_i = \chi_i$, where $\chi = (\chi_i)_{i\in[1,n]}$ are the classical thermal diffusion ratios. The diffusion matrix, the thermal diffusion factors and the thermal conductivity are the transport coefficients of the mixture. They depend on the state of the mixture, i.e., on the temperature and the species mass fractions and are evaluated as described in the next section.

The boundary conditions at the reactant stream, $x = -\infty$, read

$$Y_i(-\infty) = Y_i^{\text{u}}, \qquad i \in [1,n], \tag{6}$$

$$T(-\infty) = T^{\text{u}}, \tag{7}$$

where Y_i^{u}, $i \in [1,n]$, and T^{u} are the given species mass fractions and temperature of the unburnt gases. On the other hand, the boundary conditions for the hot stream of burnt bases at $x = +\infty$ read

$$d_x Y_i(+\infty) = 0, \qquad i \in [1,n], \tag{8}$$

$$d_x T(+\infty) = 0. \tag{9}$$

We introduce an ignition temperature T_i below which the chemical production rates vanish. Several mathematical studies have shown that the boundary value problem (1)–(9) is then well posed (Giovangigli, 1999). The ignition temperature is used to reformulate the problem over the interval $[0, +\infty)$. Upon integrating the conservation equations (1) and (2) over $(-\infty, 0)$, we derive the following boundary conditions at $x = 0$

$$T(0) - T_i = 0, \tag{10}$$

$$\rho(0)Y_i(0)U_i(0) + m(Y_i(0) - Y_i^{\mathrm{u}}) = 0, \qquad i \in [1, n], \tag{11}$$

$$\widetilde{Q}(0) + m \sum_{i\in[1,n]} Y_i^{\mathrm{u}}(h_i(0) - h_i^{\mathrm{u}}) = 0, \tag{12}$$

where we have used the notation $h_j(0) = h_j\big(T(0)\big)$ and similar notation for the other thermodynamic and transport quantities depending on the state of the mixture at $x = 0$. Using the definition of the thermal heat flux (5), the latter boundary condition reads

$$-\lambda(0)d_xT(0) + p \sum_{i\in[1,n]} X_i(0)\widetilde{\chi}_i(0)U_i(0) + m \sum_{i\in[1,n]} Y_i^{\mathrm{u}}(h_i(0) - h_i^{\mathrm{u}}) = 0. \tag{13}$$

Two important points are worth mentionning. First we note that the boundary condition (10) removes the translational invariance of the problem. In addition, the boundary conditions (10)–(12) yield the necessary and sufficient conditions for a solution on $[0, +\infty)$ to be extendable to a solution of the original problem on $(-\infty, +\infty)$. This is at variance with artificial boundary conditions imposing the temperature at an additional point $x > 0$ and which have no physical justification. Finally, we reduce the computational domain to $[0, L]$ by replacing the boundary conditions (8)–(9) for the hot stream by

$$d_xY_i(L) = 0, \qquad i \in [1, n], \tag{14}$$

$$d_xT(L) = 0. \tag{15}$$

The second type of flames considered in this paper consists of doubly premixed steady laminar flames obtained in two counterflowing symmetric jets, as illustrated in Figure 1. Our model for counterflow symmetric flames assumes a laminar, low Mach number, stagnation point flow. It is well-known that the system of two-dimensional, governing equations expressing conservation of species mass, momentum and energy

admits a similarity solution which is the solution of a one-dimensional boundary value problem. The derivation of these equations is detailed by Giovangigli (1988). In particular, using the compatibility condition at the unburnt stream, the scaled pressure gradient in the momentum equation can be evaluated in terms of the density of the unburnt stream ρ^{u}.

Let x denote the independent axial coordinate normal to the symmetry plane, y the transverse coordinate, and (u, v) the velocity components in the normal and transverse directions, respectively. We introduce the mass flow rate in the x direction given by $\tilde{u} = \rho u$ and the nondimensional transverse velocity $\tilde{v} = v/(\alpha y)$ where α denotes the strain rate imposed on the flame by the flow. The governing equations then read

$$\rho\alpha\tilde{v} + d_x\tilde{u} = 0, \tag{16}$$

$$\tilde{u}d_x\tilde{v} + \alpha(\rho\tilde{v}^2 - \rho^{\mathrm{u}}) - d_x(\eta d_x\tilde{v}) = 0, \tag{17}$$

$$\tilde{u}d_xY_i + d_x(\rho Y_iU_i) - m_i\omega_i = 0, \qquad i \in [1, n], \tag{18}$$

$$\tilde{u}c_pd_xT + d_x\widetilde{Q} + \Big(\sum_{i\in[1,n]} \rho Y_iU_ic_{pi}\Big)d_xT + \sum_{i\in[1,n]} h_im_i\omega_i = 0, \tag{19}$$

completed by the ideal gas law (3). The shear viscosity η depends on the temperature and the species mass fractions and is evaluated as described in the next section. On the other hand, the species diffusion velocities and the thermal heat flux are still given by (4)–(5).

The boundary conditions at the symmetry plane $x = 0$ read

$$\tilde{u}(0) = 0, \qquad d_x\tilde{v}(0) = 0, \tag{20}$$

$$d_xY_i(0) = 0,\ i \in [1, n], \qquad d_xT(0) = 0, \tag{21}$$

and at the unburnt stream $x = +\infty$, we have

$$\tilde{v}(+\infty) = 1, \tag{22}$$

$$Y_i(+\infty) = Y_i^{\mathrm{u}},\ i \in [1, n], \qquad T(+\infty) = T^{\mathrm{u}}, \tag{23}$$

where Y_i^{u}, $i \in [1, n]$, and T^{u} are the specified species mass fractions and temperature at the unburnt stream. Finally, we reduce the computational domain to $[0, L]$ by replacing (22)–(23) with

$$\tilde{v}(L) = 1, \tag{24}$$

$$Y_i(L) = Y_i^{\mathrm{u}},\ i \in [1, n], \qquad T(L) = T^{\mathrm{u}}. \tag{25}$$

3 DETAILED MULTICOMPONENT TRANSPORT

The transport coefficients arising in the governing equations of freely propagating and counterflow flames are the diffusion matrix $D = (D_{ij})_{i,j\in[1,n]}$, the thermal diffusion factors $\widetilde{\chi} = (\widetilde{\chi}_i)_{i\in[1,n]}$, the thermal conductivity λ, and the shear viscosity η. The diffusion matrix D is symmetric and positive definite on the hyperplane of zero sum gradients, the thermal diffusion factors satisfy $\sum_{i\in[1,n]} X_i\widetilde{\chi}_i = 0$, and we have the mass conservation relations $\sum_{i\in[1,n]} Y_i D_{ij} = 0$ for $j \in [1,n]$. All the transport algorithms considered in this work in order to evaluate D and $\widetilde{\chi}$ automatically satisfy the above physical constraints.

The transport coefficients depend on the state of the mixture, i.e., the temperature and the species mass fractions. However, the kinetic theory does not provide explicit expressions for the transport coefficients but instead linear systems which must be solved first. The transport linear systems (TLS in short) stem from an approximate solution of the linearized Boltzmann equations using a Galerkin approach based on polynomial expansions (Waldmann and Trübenbacher, 1962). The TLS read

$$\begin{cases} G\alpha = \beta, \\ \quad \alpha \in \mathcal{G}^{\perp}, \end{cases} \tag{26}$$

where G is a matrix and where α, β, and $\mathcal{G}$ are vectors. The dimension ν of the linear system is equal to the dimension of the functional space used for the polynomial expansions. The transport coefficient μ associated with (26) is typically given by the scalar product

$$\mu = \langle \alpha, \beta' \rangle, \tag{27}$$

where β' is a given vector. The matrix G and the vectors β, $\mathcal{G}$, and β' are functions of the state of the mixture and may be expressed in terms of molecular parameters. All the TLS considered in this work are detailed by Ern and Giovangigli (1994, 1998).

The mathematical structure of the TLS (26) has been obtained under very general assumptions (Ern and Giovangigli, 1994, 1996a). An important point is that we consider the TLS in their naturally constrained, singular and *symmetric* form. This is at variance with the approach of Monchick, Yun and Mason (1963) and Hirschfelder, Curtiss, and Bird (1954) which have artificially destroyed this symmetry. However, the symmetric formulation is important from a mathematical, physical, and numerical viewpoint. In particular, regarding the numerical advantages, we point out that symmetric systems can be inverted at lower computational costs, they are preferable

for iterative techniques and they lead to simpler analytic expressions. As a result, a new derivation of the TLS in symmetric form was performed by Ern and Giovangigli (1994), revealing two misprints in the paper of Monchick, Yun, and Mason.

As a consequence of the mathematical structure of the TLS, it is rigorously shown that all the transport coefficients can be expanded as convergent series. Two types of iterative methods can be considered: relaxation methods or preconditioned conjugate gradient methods. Accurate and cost-effective approximate expressions for the transport coefficients are then obtained by truncation. Numerical experiments on various flame applications have shown that one to three iterations are in general sufficient to produce approximations for the transport coefficients within less than a percent accuracy. The present multicomponent transport algorithms are implemented in a general-purpose library optimized for scalar and vector computer architectures. On scalar machines, speedups in CPU time for evaluating thermal diffusion coefficients with respect to existing software (Kee *et al.*, 1986) are as high as an order of magnitude and almost reach two orders of magnitude when vector optimization is used. For more details, we refer to Ern and Giovangigli (1996b, 1996c).

For evaluating the diffusion matrix, the most practical TLS is of size $\nu = n$ and involves the system matrix Δ given by

$$\Delta_{ii} = \sum_{\substack{j\in[1,n]\\ j\neq i}} \frac{X_i X_j}{\mathcal{D}_{ij}}, \qquad i \in [1,n], \tag{28}$$

$$\Delta_{ij} = -\frac{X_i X_j}{\mathcal{D}_{ij}}, \qquad i,j \in [1,n], \quad i \neq j, \tag{29}$$

where $\mathcal{D}_{ij}$ is the binary diffusion coefficients of species pair $\{i,j\}$. Following the ideas of Giovangigli (1991) and Ern and Giovangigli (1994, 1995), we obtain approximate expressions for the diffusion matrix in the form

$$D^{[k]} = \sum_{l=0}^{k} (PT)^l P M^{-1} P^t, \tag{30}$$

where P is the projector given by $P_{ij} = \delta_{ij} - Y_j$, for $i,j \in [1,n]$, M the diagonal matrix $M = \mathrm{diag}(X_1/D_1^*, \ldots, X_n/D_n^*)$ with

$$D_i^* = \frac{1 - Y_i}{\sum_{j\neq i} X_j/\mathcal{D}_{ij}}, \qquad i \in [1,n], \tag{31}$$

and $T = I - M^{-1}\Delta$. Note that the spectral radius of T is unity whereas the spectral radius of the *projected* matrix PT is strictly lower than unity. We also point out that

all the approximate diffusion matrices $D^{[k]}$ satisfy the important physical properties of symmetry, positive definiteness on the physical hyperplane of zero sum gradients, and mass conservation.

The first term in the series expansion, namely $D^{[0]} = PM^{-1}P^t$, corresponds to the Hirschfelder-Curtiss approximation (1949) with a mass correction diffusion velocity (Jones and Boris, 1981, Oran and Boris, 1981). The second term in the series expansion, namely $D^{[1]}$, provides a new approximate expression for the diffusion matrix. It was first introduced by Giovangigli (1991) and given explicitly by Ern *et al.* (1996) when modelling chemical vapor deposition reactors. It may be written in the form $D^{[1]} = P\mathcal{T}P^t$ with the matrix $\mathcal{T}$ given by

$$\mathcal{T}_{ii} = \frac{D_i^*}{X_i}(1 + Y_i), \qquad i \in [1, n], \tag{32}$$

$$\mathcal{T}_{ij} = \frac{D_i^* D_j^*}{\mathcal{D}_{ij}}, \qquad i, j \in [1, n], \quad i \neq j. \tag{33}$$

We also point out that it is interesting from a numerical viewpoint to consider the modified diffusion matrix $D^{[k]} + aU \otimes U$ where a is an arbitrary positive quantity and U the vector $U = (1, \ldots, 1)$. The additional term removes artificial singularities in the discretized conservation equations (Giovangigli, 1990).

For evaluating the thermal conductivity and the thermal diffusion factors, we consider a TLS of size $\nu = n$. This system has been introduced by Ern and Giovangigli (1994) and results from polynomial expansions in the total energy of the molecules. It yields accurate expressions for the associated transport coefficients and is also of smaller size than the standard TLS of size $\nu = 2n$, thus reducing the computational costs. Accurate and cost-effective approximations for the thermal conductivity and the thermal diffusion factors are obtained after three conjugate gradient iterations.

For evaluating the shear viscosity, we consider the TLS of size $\nu = n$. An accurate and cost-effective approximation for the shear viscosity is obtained after one conjugate gradient iteration. It is worthwhile to notice that this approximation is already an order of magnitude more accurate than the Wilke approximation, but requires less CPU time to be evaluated.

In order to investigate the impact of thermal diffusion and multicomponent mass diffusion on flame structure, we consider three different models for the species diffusion velocities. Model I is the most accurate, while model III is the least accurate and also the most frequently used in previous work. Model II is an hybrid model introduced for comparison purposes. Specifically, we consider

Model I: "Multicomponent mass and thermal diffusion"

$$U_i = -\sum_{j\in[1,n]} D_{ij}^{[1]}(d_x X_j + X_j \widetilde{\chi}_j d_x \log T), \qquad i \in [1,n]. \tag{34}$$

Model II: "Multicomponent mass and no thermal diffusion"

$$U_i = -\sum_{j\in[1,n]} D_{ij}^{[1]} d_x X_j, \qquad i \in [1,n]. \tag{35}$$

Model III: "Diagonal mass and no thermal diffusion"

$$U_i = -\sum_{j\in[1,n]} D_{ij}^{[0]} d_x X_j, \qquad i \in [1,n]. \tag{36}$$

Note that it is also possible to consider a "diagonal mass and thermal diffusion" model for the species diffusion velocities upon writing $U_i = -\sum_{j\in[1,n]} D_{ij}^{[0]}(d_x X_j + X_j \widetilde{\chi}_j d_x \log T)$, for $i \in [1,n]$. This model is not further considered here since the computational overhead for evaluating $D^{[1]}$ instead of $D^{[0]}$ is marginal if the thermal diffusion factors are also evaluated. In addition, this model may lead to numerical instabilities for two-dimensional bunsen flames (Ern and Giovangigli, 1998).

4 METHOD OF SOLUTION

The solution method combines a pseudo-arclength continuation procedure, Newton iterations and global adaptive gridding, as detailed by Giovangigli and Smooke (1987, 1989, 1992). For both freely propagating and counterflow flames, the set of governing equations and boundary conditions reduces after discretization to a system of the form

$$\mathcal{F}(\mathcal{Z}, \gamma) = 0, \tag{37}$$

where $\mathcal{Z}$ is the discrete solution vector and γ any physical parameter of the system, e.g., the equivalence ratio ϕ or the strain rate α. For freely propagating flames, we introduce the additional dummy equation $d_x m = 0$ in order to simplify the structure of the Jacobian matrix. The solution vector has then components given by $(Y_1, \ldots, Y_n, T, m)$. On the other hand, for counterflow flames, the solution vector has components $(\tilde{u}, \tilde{v}, Y_1, \ldots, Y_n, T)$.

Because of the presence of turning points, the one-dimensional manifold $(\mathcal{Z}, \gamma)$ cannot be parametrized as $(\mathcal{Z}(\gamma), \gamma)$. The solutions $(\mathcal{Z}, \gamma)$ are then obtained using a

pseudo-arclength continuation method. A new parameter s is introduced in order to reparametrize the manifold into $\big(\mathcal{Z}(s), \gamma(s)\big)$ in such a way that s approximates the arclength of the solution branch in a given phase space. Note that this reparametrization suppresses the singularities due to simple turning points and also yields better conditioned Jacobian matrices. The new system of discrete governing equations now reads

$$\mathcal{H}(\mathcal{Z}, \gamma, s) = 0. \tag{38}$$

Starting from a previously obtained solution $\big(\mathcal{Z}(s_0), \gamma(s_0)\big)$, the solution branch is extended using a first-order Euler predictor followed by an implicit correction step involving Newton iterations. Thanks to the structure of the Jacobian matrix, an optimized block-tridiagonal solver can be used to solve the associated linear systems. In addition, for the sake of computational efficiency, the Jacobian matrix is evaluated numerically using vector function evaluations and highly optimized libraries for thermochemistry (Giovangigli and Darabiha, 1988) and multicomponent transport (Ern and Giovangigli, 1996c).

Finally, in order to resolve the high activity regions in the flame and to optimize the number of grid points along the solution branch, a new adaptive mesh is generated after each continuation step by equidistributing a weight function involving the gradient and curvature of all the components of the numerical solution. For more details, we refer to Giovangigli and Smooke (1989).

5 FREELY PROPAGATING FLAMES

In this section we apply the physical model and the numerical method discussed in the previous sections in order to obtain the flame peak temperature and the flame speed versus equivalence ratio for freely propagating hydrogen/air and methane/air flames. For hydrogen/air flames, we consider a finite rate, chemical reaction mechanism involving the $n = 9$ species H_2, O_2, N_2, H_2O, H, O, OH, HO_2, and H_2O_2 participating in 19 elementary reactions (Giovangigli and Smooke, 1992). For methane/air flames, we consider a finite rate, chemical reaction mechanism including propane chemistry and involving $n = 33$ species participating in 126 elementary reactions (Darabiha *et al.*, 1988). The length of the computational domain is set to $L = 30$ cm. We consider atmospheric flames with unburnt gases at temperature $T^{\mathrm{u}} = 300$ K and an ignition temperature of $T_i = 301$ K.

Plane premixed laminar flames have been investigated using continuation methods by Giovangigli and Smooke (1992). Extinction of such flames can be obtained experimentally by adjusting the reactant concentrations in the unburnt stream. By varying the equivalence ratio, it is possible to decrease the heat released by chemical reactions to a level where external heat losses become predominant and the flame extinguishes. Although heat losses are important theoretically, the actual value of the heat loss rate has a minor impact on the equivalence ratio at extinction over practically interesting operating conditions (Williams, 1985). Since no heat losses are considered here, no physically relevant turning points in the equivalence ratio are obtained numerically. As the equivalence ratio approaches the rich flammability limit, the flame speed is reduced considerably and the flame thickness becomes larger. The flame eventually occupies all the computational domain and a turning point in ϕ is passed. The continuation procedure then generates a branch of unstable flames pressed against the boundary $x = L$. Once the lean flammability limit is passed, the flame thickness decreases and a classical flame structure is again recovered. For more details, we refer to Giovangigli and Smooke (1992). Since only model III for the species diffusion velocities was considered by these authors, our goal is now to evaluate the impact of the more accurate models I and II.

Considering first hydrogen/air flames, the left part of Figure 2 presents the laminar flame speed as a function of the equivalence ratio obtained using models I, II, and III. Comparing first models II and III, we can see that using the more accurate diffusion matrix $D^{[1]}$ instead of $D^{[0]}$ results in predicting slightly lower flame speeds for all the equivalence ratios. The differences in computed flame speeds are, however, not very important. A comparison of models I and II shows on the other hand the more important role played by thermal diffusion. Indeed, for lean flames, the flame velocity is significantly lower when thermal diffusion is included in the model. For such flames, the thermal diffusion factor of most radicals is negative throughout the flame. As a result, when thermal diffusion is included, active radicals are less prone to diffuse into the cold region and flame propagation is, therefore, slower. However, for rich flames, the zoom shown in the right part of Figure 2 reveals that the flame speed is slightly higher when thermal diffusion is included in the model. This result differs from the one reported by Warnatz (1982) where thermal diffusion was included only for the light species, i.e., atomic and molecular hydrogen. The increase in flame speed can only be obtained with a detailed transport model. Indeed, as discussed below through a detailed analysis of a rich flame structure, the thermal diffusion factor of O and OH changes sign abruptly inside the flame front. We also point out that although the increase in flame speed is

not very significant since the relative changes are of the order of a few percent, it has some impact on the structure of multidimensional rich hydrogen/air bunsen flames, as discussed by Ern and Giovangigli (1998). Finally, it is worthwhile to point out that while the flame speed is sensitive to the accuracy of the multicomponent transport model, this is not the case for the peak temperature which was found to be practically the same, independently of models I–III.

We now discuss into more detail two flame structures. We consider a lean flame with 20% hydrogen in mole fraction in the unburnt gases and a rich flame with 70% hydrogen in mole fraction. These flames correspond to equivalence ratios of $\phi = 0.59$ and $\phi = 5.55$, respectively. Turning our attention to the lean flame first, we present in Figure 3 the thermal diffusion factor of species H_2, H, O, OH, and H_2O_2 throughout the flame. For completeness, the figure also contains a scaled temperature profile, the actual temperature varying between 300 and 1820 K. It is seen that except for the heavy species H_2O_2, all the thermal diffusion factors are negative and thus the flame speed should be indeed smaller when thermal diffusion is included in the model. The impact of thermal diffusion on the species and temperature profiles is illustrated in Figure 4. Important changes can be observed. For instance, at $x = 0.4$ mm, the temperature is 1040 K with model I and 100 K higher with model II. The major species profiles also exhibit important variations. The O_2 and N_2 profiles show that these heavy species indeed diffuse into the cold zone when thermal diffusion is included, while H_2 diffuses into the hot zone. Significant variations between models I and II are also observed in all the radicals profiles. Focusing next on the rich flame, we present in Figure 5 the thermal diffusion factor of species H_2, H, O, OH, and H_2O_2 throughout the flame along with a scaled temperature profile, the actual temperature varying between 300 and 1340 K. It is seen that the thermal diffusion factor for radicals O and OH is negative in the hot zone, positive in the cold zone, and, therefore, does not promote diffusion into the cold zone. As a result, the flame propagation velocity is actually slightly higher when thermal diffusion is included in the model. Finally, in Figure 6, we compare the species and temperature profiles obtained with models I and II. Changes in the temperature are much less important than those observed for the lean flame. On the other hand, thermal diffusion yields higher concentrations of O_2 and N_2 close to the cold zone, as to be expected. The H_2 profile exhibits a very interesting phenomenon. Indeed, although thermal diffusion as a single effect tends to drive H_2 towards the hot flame region, the nonlinear coupling between transport and chemistry results in the opposite effect, i.e., the H_2 concentration is actually lower in the hot flame region when thermal diffusion is included in the model. Finally, significant variations in the radicals profiles

are observed from Figure 6 when model I is used instead of model II.

Considering next methane/air flames, Figure 7 presents the computed flame speed as a function of equivalence ratio for models I–III. We observe practically no variations in flame speed between the results of models II and III. On the other hand, thermal diffusion tends to lower slightly the flame propagation velocity, the impact being the most important for stoichiometric and slightly rich flames. Indeed, the Soret effect reduces the diffusion of chemical radicals in the active reaction zone thus acting against flame propagation.

6 COUNTERFLOW FLAMES

In this section we discuss our numerical results for counterflow hydrogen/air and methane/air flames. We use the same chemical mechanism as in the previous section for hydrogen/air flames, whereas for methane/air flames we consider a C1-chain reaction mechansim involving $n = 16$ species participating in 46 elementary reactions (Ern *et al.*, 1995). We apply the pseudo-arclength continuation procedure discussed in Section 4 in order to predict the peak temperature in the flames as a function of either the strain rate or the equivalence ratio. In all the calculations, we consider atmospheric flames with the length of the computational domain set to $L = 3$ cm and the temperature of the unburnt gases to $T^{\mathrm{u}} = 300$ K. Extinction of strained premixed flames with complex chemistry has been investigated numerically using continuation methods by Giovangigli and Smooke (1987). Since these authors only used model III for the species diffusion velocities, our goal is now to evaluate the impact of models I–III on the flame temperature response curves to varying the strain rate or the equivalence ratio.

We consider first the results for hydrogen/air flames. In Figure 8 we present the peak temperature as a function of strain rate for a lean flame with 20 percent hydrogen in mole fraction. Starting at a value of $\alpha = 500$ s^{-1}, we first note an increase in the peak temperature. This effect can be attributed to the diffusion of hydrogen (the deficient reactant) from the unburnt mixture into the reaction zone, causing additional heat release larger than the conductive heat losses. As the strain rate continues to increase above 2000 s^{-1}, the temperature starts to decrease and the flame is pressed against the stagnation plane until incomplete combustion due to decreased residence times eventually extinguishes the flame. We also point out that the peak temperature of the freely propagating 20 percent hydrogen/air flame is about 1820 K. Hence, we

observe in the present strained flames Lewis number effects between 20 and 80 K, in qualitative agreement with the theory of Libby and Williams (1984).

Figure 8 also illustrates the impact of detailed multicomponent transport on model predictions. A comparison of the numerical results obtained with models II and III first shows that the use of the more accurate matrix $D^{[1]}$ has only a minor influence on the peak temperature. Peak temperatures are globally lower when this matrix is considered. A comparison of models I and II–III reveals, however, a more important role played by thermal diffusion. Inclusion of thermal diffusion leads to higher peak temperatures. For instance, at a strain rate of 2000 s^{-1}, the peak temperature is 1870 K with model II and 1910 K with model I. In Figure 9 we next consider peak temperature versus strain rate for a rich flame with 70 percent hydrogen in mole fraction. We observe a strong impact of thermal diffusion on the extinction limit, which is predicted to be $\alpha = 1691$ s^{-1} with Model I and $\alpha = 2309$ s^{-1} with Model II, thus 36% higher. It is also interesting to notice that the effect of thermal diffusion is the opposite to the one observed for lean flames. Indeed, the peak temperature is now lower when model I is used. This phenomenon can be interpreted using the theoretical work of Libby *et al.* (1983) and Libby and Williams (1984) on strained premixed laminar flames with nonunity Lewis number. For lean hydrogen flames, thermal and mass diffusion of hydrogen occurs in the same direction, towards the hot flame front. Thus, the inclusion of thermal diffusion lowers the overall Lewis number for hydrogen and enhances the effect of nonunity Lewis number: the flame temperature gets higher. For rich flames, thermal and mass diffusion for oxygen act in the opposite direction and inclusion of thermal diffusion enhances the overall Lewis number for oxygen: the flame temperature is now lower.

Figure 10 next shows the variation of the peak temperature as a function of equivalence ratio for a fixed strain rate of $\alpha = 1500$ s^{-1}. While the differences obtained with models II and III are not very important, thermal diffusion has a stronger impact, especially on the rich extinction limit. Indeed this limit is predicted to be 4.09 with model I and 4.30 with model II. Some changes are also observed for the lean flames. For instance, the lean extinction limit is found to be 0.22 with model I and 0.24 with model II. For lean flames, peak temperatures at a given strain rate are higher when thermal diffusion is included so that flames with thermal diffusion can support smaller values of the equivalence ratio before extinction.

We now discuss our numerical results for methane/air flames. Figure 11 presents the peak flame temperature as a function of the strain rate for a stoichiometric flame obtained with models I–III. Since the Lewis number for methane is about unity, we

anticipate a monotonic decrease in temperature as a function of the strain rate. As the strain rate is further increased, the flame is pressed against the symmetry plane and eventually extinguishes. The extinction limit is slightly higher when thermal diffusion is included. For instance, the strain rate at extinction is $\alpha = 1921$ s^{-1} with Model I and $\alpha = 1881$ s^{-1} with Model III. Finally, we consider in Figure 12 the variation of the flame peak temperature as a function of equivalence ratio for a fixed strain rate of $\alpha = 1000$ s^{-1}. It is seen that thermal diffusion has some impact on both the lean and the rich extinction limits, the major differences being observed between model I and II. The rich extinction limit is $\phi = 1.17$ with model I and $\phi = 1.21$ with model II. On the other hand, the lean extinction limit is $\phi = 0.70$ with model I and $\phi = 0.72$ with model II.

7 CONCLUSIONS

In this paper we have derived a physical model with complex chemical kinetics and detailed multicomponent transport and used adaptive continuation techniques in order to investigate computationally freely propagating and counterflow premixed steady flames. We have investigated quantitatively the importance of modeling the species diffusion velocities accurately. For freely propagating lean hydrogen/air flames, the flame speed is lower when thermal diffusion is included in the model. However, for rich flames, flame propagation is slightly faster as a result of thermal diffusion factors of some radicals changing sign at the flame front. For freely propagating methane/air flames, thermal diffusion has no significant impact on flame speed and flame structure. For counterflow flames, both methane and hydrogen, extinction limits in terms of either strain rate or equivalence ratio are sensitive to multicomponent transport. The effects are more pronounced for hydrogen flames, especially the rich flames, where neglecting thermal diffusion can lead to overprediction of the strain rate at extinction by 36%.

Acknowledgments. The authors are thankful to M.D. Smooke for fruitful discussions and to the 'Institut du Développement des Ressources Informatiques et Scientifiques' (IDRIS, France) for providing part of the computational resources.

REFERENCES

Darabiha, N., Candel, S., Giovangigli, V., and Smooke, M. D. (1988) Extinction of strained premixed propane/air flames with complex chemistry. *Combust. Sci. Tech.* **80**, 267–284.

Dixon-Lewis, G. (1968) Flame structure and flame reaction kinetics, II: transport phenomena in multicomponent systems. *Proc. Roy. Soc. London*, **A307**, 111–135.

Ern, A., Douglas, C. C., and Smooke, M. D. (1995) Detailed chemistry modeling of laminar diffusion flames on parallel computers. *Int. J. Supercomput. Appl.* **9**, 167–186.

Ern, A. and Giovangigli, V. (1994) *Multicomponent Transport Algorithms*, Springer-Verlag, Heidelberg, Lecture Notes in Physics, New Series Monographs, **m 24**.

Ern, A. and Giovangigli, V. (1995) Fast and accurate multicomponent transport property evaluation. *J. Comput. Phys.* **120**, 105–116.

Ern, A. and Giovangigli, V. (1996a) The structure of transport linear systems in dilute isotropic gas mixtures. *Phys. Rev. E*, **53**, 485–492.

Ern, A. and Giovangigli, V. (1996b) Optimized transport algorithms for flame codes. *Combust. Sci. and Tech.* **118**, 387–395.

Ern, A. and Giovangigli, V. (1996c) EGlib server with user's manual [http://www.cmap.polytechnique.fr/www.eglib].

Ern, A. and Giovangigli, V. (1998) Thermal diffusion effects in hydrogen/air and methane/air flames. *Combust. Theory and Model.* **2**, 349–372.

Ern, A., Giovangigli, V., and Smooke, M. D. (1996) Numerical study of a three-dimensional chemical vapor deposition reactor with detailed chemistry. *J. Comput. Phys.* **126**, 21–39.

Ferziger, J. H. and Kaper, H. G. (1972) *Mathematical Theory of Transport Processes in Gases*, North Holland, Amsterdam.

García-Ybarra, P., Nicoli, C., and Clavin, P. (1984) Soret and dilution effects on premixed flames. *Combust. Sci. Tech.* **42**, 87–109.

Giovangigli, V. (1988) *Structure et extinction de flammes laminaires prémélangées*, Thèse de Doctorat d'Etat, Université Paris VI.

Giovangigli, V. (1990) Mass conservation and singular multicomponent diffusion algorithms. *Impact Comput. Sci. Eng.* **2**, 73–97.

Giovangigli, V. (1991) Convergent iterative methods for multicomponent diffusion. *Impact Comput. Sci. Eng.* **3**, 244–276.

Giovangigli, V. (1999) Plane laminar flames with multicomponent transport and complex chemistry. *Math. Model. Meth. Appl. Sci.* **9** in press.

Giovangigli, V. and Darabiha, N. (1988) Vector computers and complex chemistry combustion. In Brauner, C. and Schmidt-Lainé, C., (Eds.) *Mathematical Modeling in Combustion and Related Topics*, Martinus Nijhoff, Dordrecht, NATO Adv. Sci. Inst. Ser. E, Vol. 140, pp. 491–503.

Giovangigli, V. and Smooke, M. D. (1987) Extinction of strained premixed laminar flames with complex chemistry. *Combust. Sci. and Tech.* **53**, 23–49.

Giovangigli, V. and Smooke, M. D. (1989) Adaptive continuation algorithms with application to combustion problems. *Appl. Numer. Math.* **5**, 305–331.

Giovangigli, V. and Smooke, M. D. (1992) Application of continuation methods to plane premixed laminar flames. *Comb. Sci. and Tech.* **87**, 241–256.

Greenberg, J. B. (1980) On the prediction of thermal diffusion effects in laminar one-dimensional flames. *Combust. Sci. Tech.* **24**, 83–88.

Hancock, R. D., Schauer, F. R., Lucht, R. P., Katta, V. R., and Hsu, K. Y. (1996) Thermal diffusion effects and vortex-flame interactions in hydrogen jet diffusion flames, Twenty-Sixth Symposium (International) on Combustion, The Combustion Institute, pp. 1087–1093.

Heimerl, J. M. and Coffee, T. P. (1982) Results of a study of several transport algorithms for premixed, laminar steady-state flames, In Peters, N. and Warnatz, J., (Eds.) *Numerical Methods in Laminar Flame Propagation*, Vieweg, Braunschweig, pp. 71–86.

Hirschfelder, J. O. and Curtiss, C. F. (1949) Flame propagation in explosive gas mixtures, Third Symposium (International) on Combustion, The Combustion Institute, pp. 121–127.

Hirschfelder, J. O., Curtiss, C. F., and Bird, R. B. (1954) *Molecular Theory of Gases and Liquids*, Wiley, New York.

Jones, W. W. and Boris, J. P. (1981) An algorithm for multispecies diffusion fluxes. *Comput. Chem.* **5**, 139–146.

Kee, R. J., Dixon-Lewis, G., Warnatz, J., Coltrin, M. E., and Miller, J. A. (1986) A Fortran computer code package for the evaluation of gas-phase multicomponent transport properties, SANDIA National Laboratories Report, SAND86-8246.

Libby, P. A., Liñán, A. and Williams, F. A. (1983) Strained premixed laminar flames with nonunity Lewis numbers. *Combust. Sci. Tech.* **34**, 257–293.

Libby, P. A. and Williams, F. A. (1984) Strained premixed laminar flames with two reaction zones. *Combust. Sci. Tech.* **37**, 221–252.

Monchick, L., Yun, K. S., and Mason, E. A. (1963) Formal kinetic theory of transport phenomena in polyatomic gas mixtures. *J. Chem. Phys.* **39**, 654–669.

Oran, E. S. and Boris, J. P. (1981) Detailed modeling of combustion systems. *Prog. Energy Combust. Sci.* **7**, 1–72.

Popp, P. and Baum, M. (1997) Analysis of wall heat fluxes, reaction mechanism, and unburnt hydrocarbons during the head-on quenching of a laminar methane flame. *Combust. Flame*, **108**, 327–348.

Waldmann, L. and Trübenbacher, E. (1962) Formale kinetische Theorie von Gasgemischen aus anregbaren Molekülen. *Zeitschr. Naturforschg.* **17a**, 363–376.

Warnatz, J. (1982) Influence of transport models and boundary conditions on flame structure, In Peters, N. and Warnatz, J., (Eds.) *Numerical Methods in Laminar Flame Propagation*, Vieweg, Braunschweig, pp. 87-111.

Williams, F. A. (1985) *Combustion Theory*, Benjamin/Cummings Pub. Co.

FIGURE CAPTIONS

Figure 1. Illustration of a symmetric counterflow flame.

Figure 2. Left: flame speed (cm/s) versus equivalence ratio for freely propagating hydrogen/air flames; comparison of three models for the species diffusion velocities. Right: zoom for rich flames.

Figure 3. Thermal diffusion factors of several chemical species and scaled temperature profile for a lean freely propagating hydrogen/air flame with 20 percent H_2 in mole fraction.

Figure 4. Chemical species mole fraction and temperature profiles obtained with and without thermal diffusion (for convenience, the N_2 mole fraction is scaled by a factor of 4); lean freely propagating hydrogen/air flame with 20 percent H_2 in mole fraction.

Figure 5. Thermal diffusion factors of several chemical species and scaled temperature profile for a rich freely propagating hydrogen/air flame with 70 percent H_2 in mole fraction.

Figure 6. Chemical species mole fraction and temperature profiles obtained with and without thermal diffusion; rich freely propagating hydrogen/air flame with 70 percent H_2 in mole fraction.

Figure 7. Flame speed (cm/s) versus equivalence ratio for freely propagating premixed methane/air flames; comparison of three models for the species diffusion velocities.

Figure 8. Flame temperature (K) versus strain rate (s^{-1}) for lean counterflow hydrogen/air flames with 20 percent hydrogen in mole fraction.

Figure 9. Flame temperature (K) versus strain rate (s^{-1}) for rich counterflow hydrogen/air flames with 70 percent hydrogen in mole fraction.

Figure 10. Flame temperature (K) versus equivalence ratio for counterflow hydrogen/air flames at a strain rate of 1500 s^{-1}.

Figure 11. Flame temperature (K) versus strain rate (s^{-1}) for stoichiometric counterflow methane/air flames.

Figure 12. Flame temperature (K) versus equivalence ratio for counterflow premixed methane/air flames at a strain rate of 1000 s^{-1}.

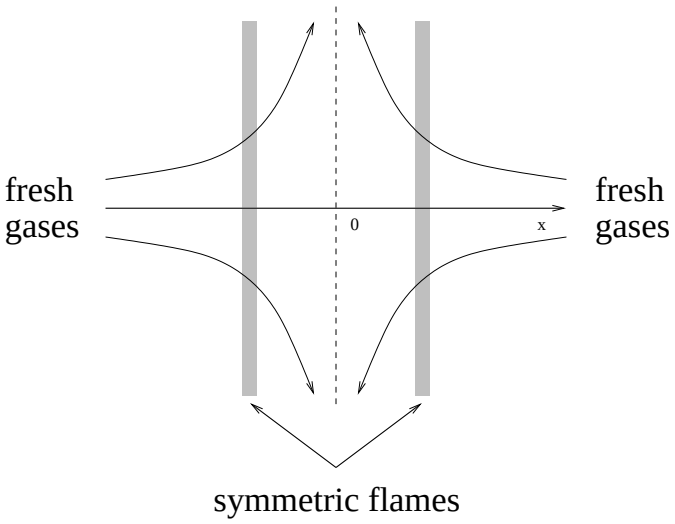

Figure 1

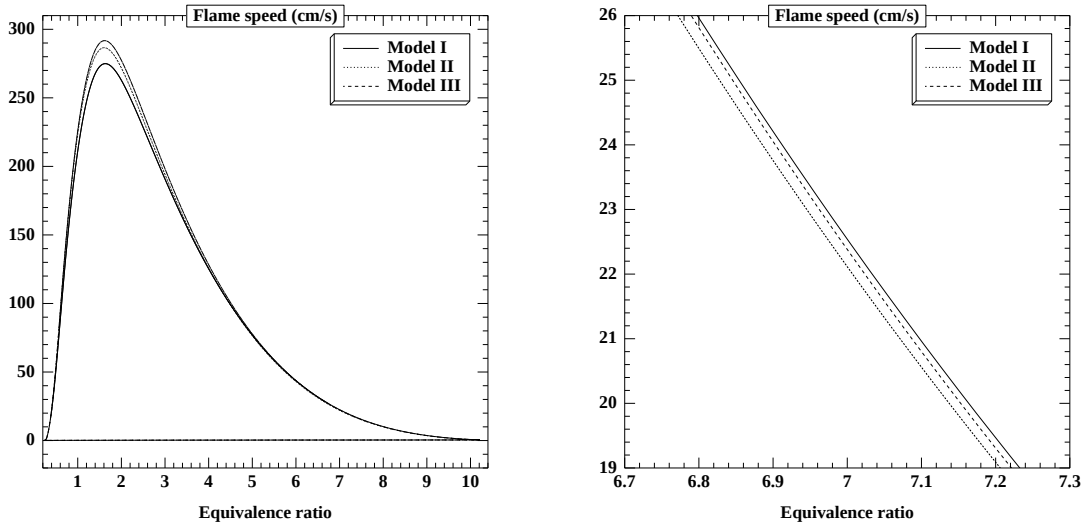
Flame speed (cm/s)
Model I
Model II
Model III
300
250
200
150
100
50
0
1
2
3
4
5
6
7
8
9
10
Equivalence ratio
Flame speed (cm/s)
Model I
Model II
Model III
26
25
24
23
22
21
20
19
6.7
6.8
6.9
7
7.1
7.2
7.3
Equivalence ratio

Figure 2

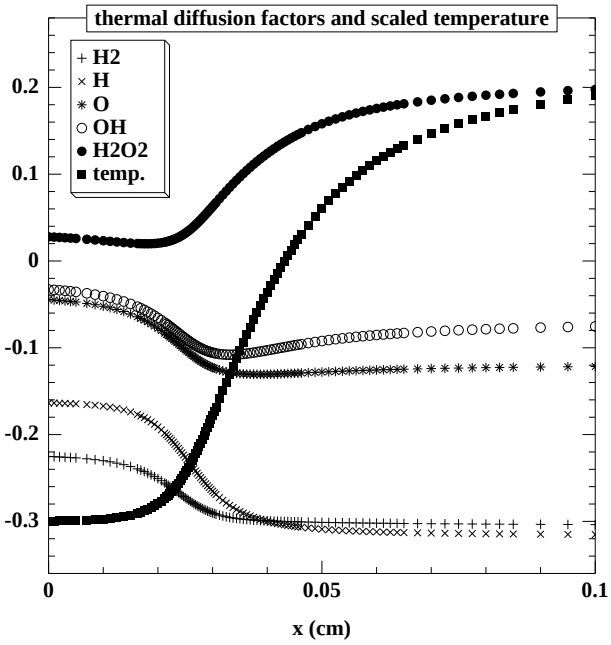
thermal diffusion factors and scaled temperature
H2
H
O
OH
H2O2
temp.
0.2
0.1
0
-0.1
-0.2
-0.3
0
0.05
0.1
x (cm)

Figure 3

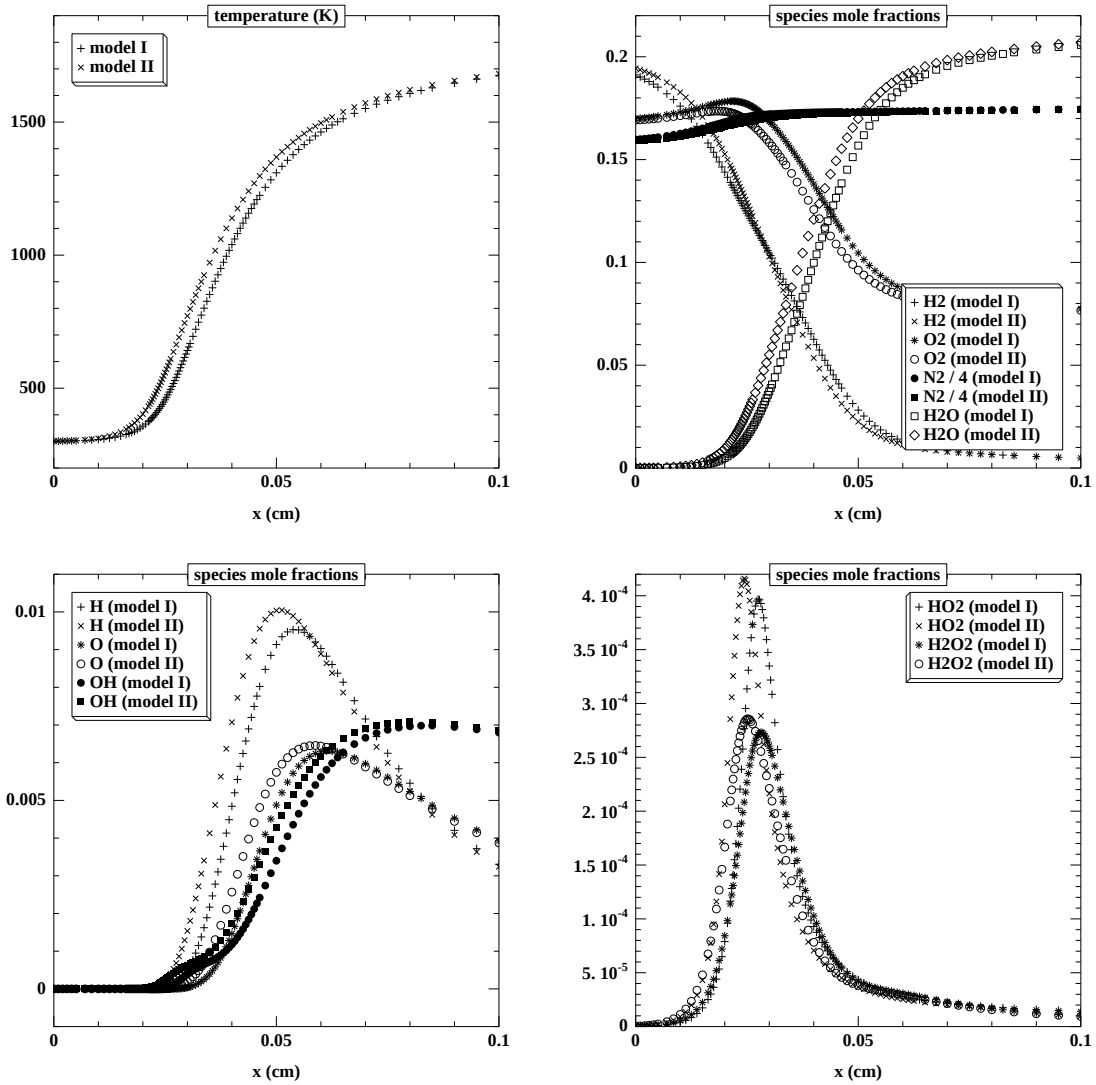
temperature (K)
model I
model II
1500
1000
500
0
0.05
0.1
x (cm)
species mole fractions
0.2
0.15
0.1
0.05
H2 (model I)
H2 (model II)
O2 (model I)
O2 (model II)
N2 / 4 (model I)
N2 / 4 (model II)
H2O (model I)
H2O (model II)
species mole fractions
0.01
0.005
H (model I)
H (model II)
O (model I)
O (model II)
OH (model I)
OH (model II)
species mole fractions
4. 10-4
3.5 10-4
3. 10-4
2.5 10-4
2. 10-4
1.5 10-4
1. 10-4
5. 10-5
HO2 (model I)
HO2 (model II)
H2O2 (model I)
H2O2 (model II)

Figure 4

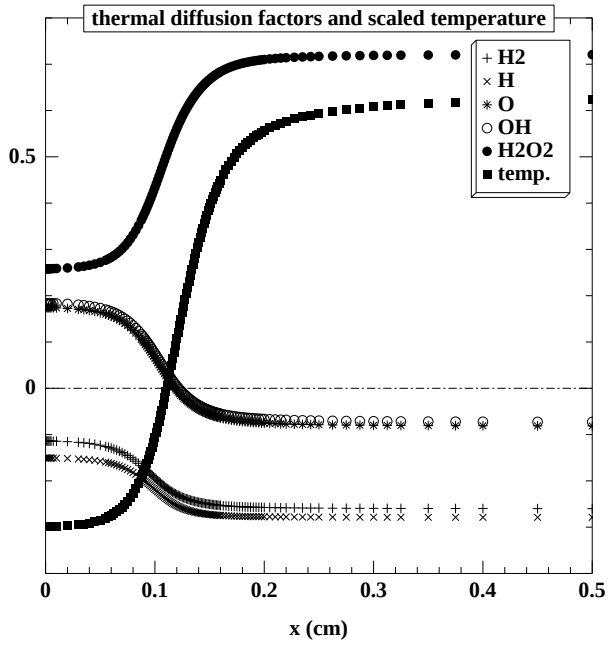
thermal diffusion factors and scaled temperature
H2
H
O
OH
H2O2
temp.
0.5
0
0
0.1
0.2
0.3
0.4
0.5
x (cm)

Figure 5

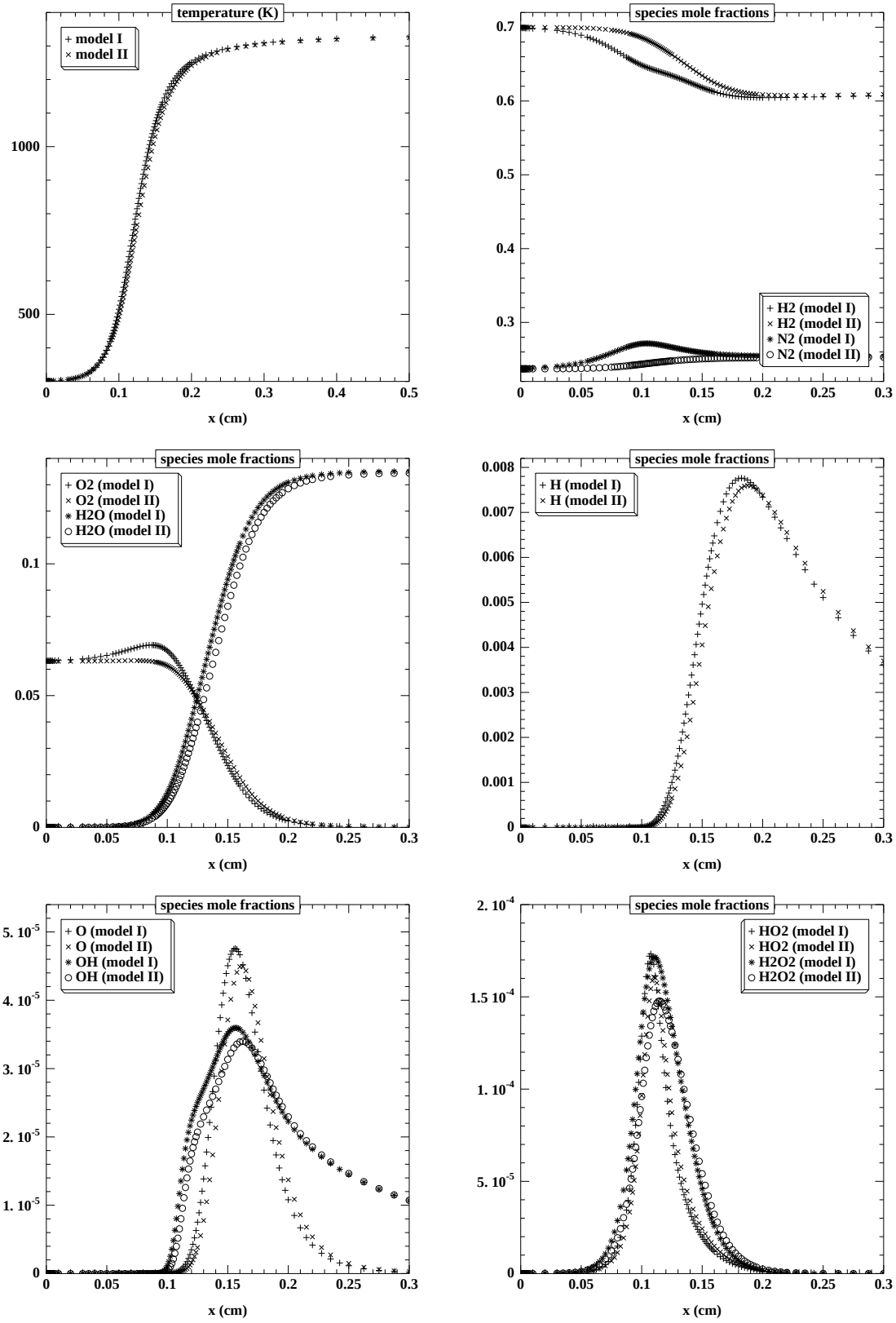
temperature (K)
+ model I
× model II
1000
500
0
0.1
0.2
0.3
0.4
0.5
x (cm)
species mole fractions
0.7
0.6
0.5
0.4
0.3
+ H2 (model I)
× H2 (model II)
∗ N2 (model I)
○ N2 (model II)
0
0.05
0.1
0.15
0.2
0.25
0.3
x (cm)
species mole fractions
+ O2 (model I)
× O2 (model II)
∗ H2O (model I)
○ H2O (model II)
0.1
0.05
0
x (cm)
species mole fractions
+ H (model I)
× H (model II)
0.008
0.007
0.006
0.005
0.004
0.003
0.002
0.001
0
x (cm)
species mole fractions
+ O (model I)
× O (model II)
∗ OH (model I)
○ OH (model II)
5. 10-5
4. 10-5
3. 10-5
2. 10-5
1. 10-5
0
x (cm)
species mole fractions
+ HO2 (model I)
× HO2 (model II)
∗ H2O2 (model I)
○ H2O2 (model II)
2. 10-4
1.5 10-4
1. 10-4
5. 10-5
0
x (cm)

Figure 6

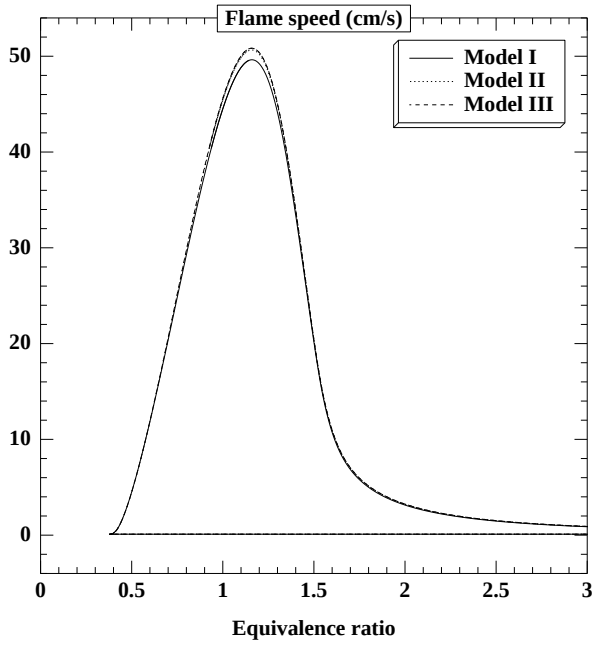
Flame speed (cm/s)
Model I
Model II
Model III
50
40
30
20
10
0
0
0.5
1
1.5
2
2.5
3
Equivalence ratio

Figure 7

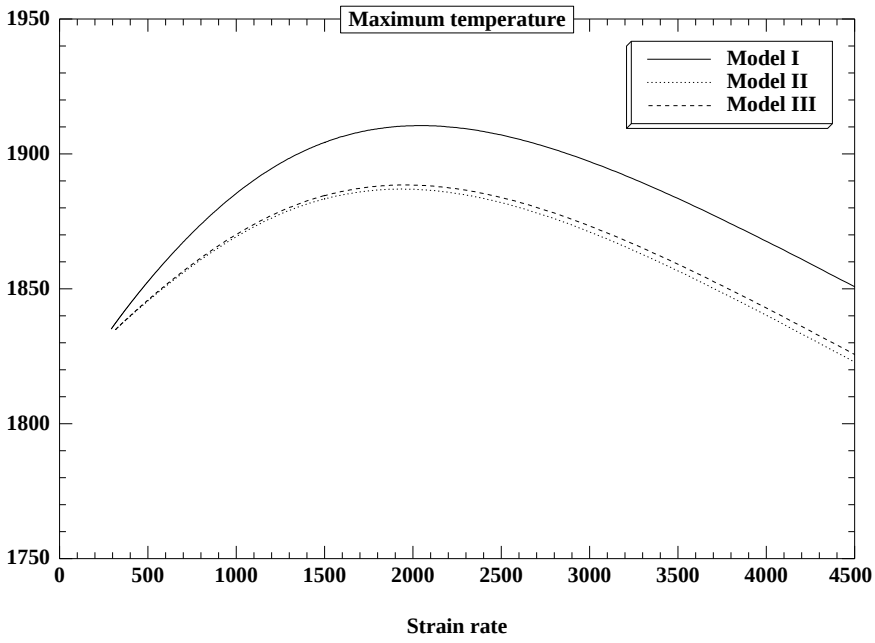
Maximum temperature
Model I
Model II
Model III
1950
1900
1850
1800
1750
0
500
1000
1500
2000
2500
3000
3500
4000
4500
Strain rate

Figure 8

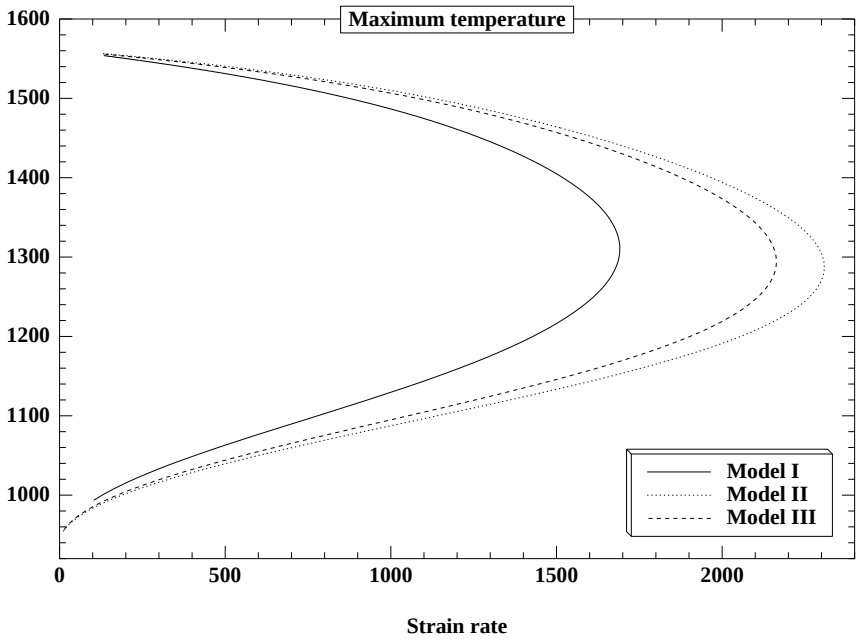
Maximum temperature
1600
1500
1400
1300
1200
1100
1000
0
500
1000
1500
2000
Strain rate
Model I
Model II
Model III

Figure 9

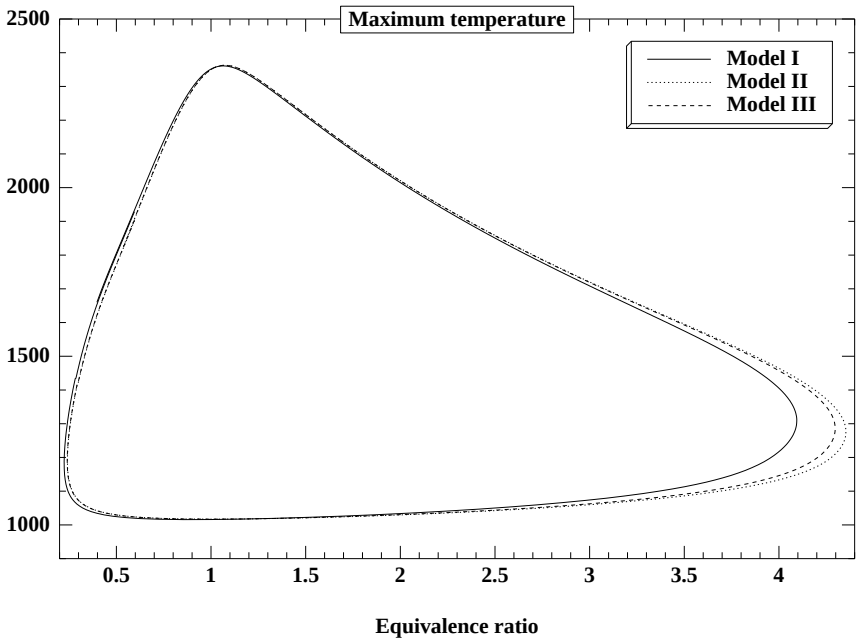
Maximum temperature
Model I
Model II
Model III
2500
2000
1500
1000
0.5
1
1.5
2
2.5
3
3.5
4
Equivalence ratio

Figure 10

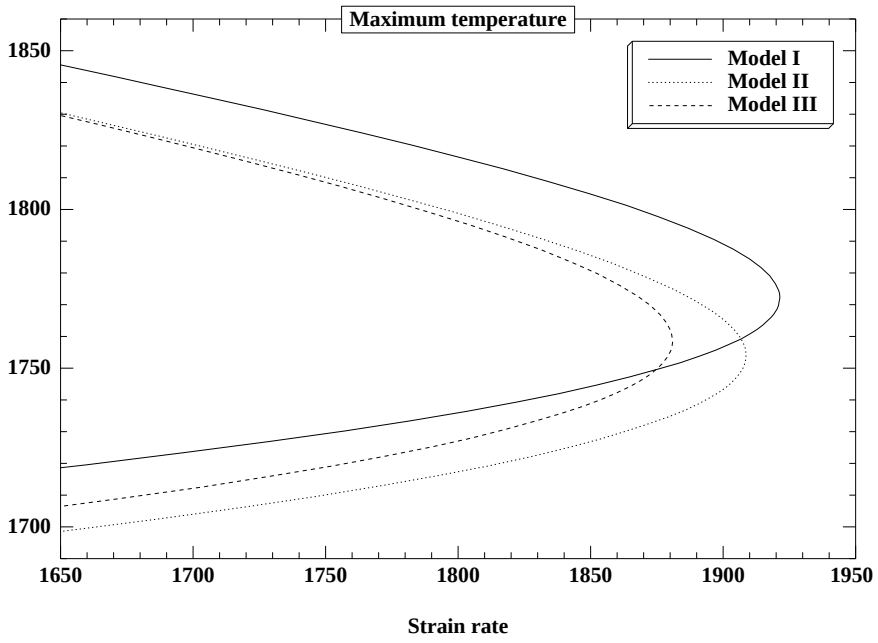
Maximum temperature
Model I
Model II
Model III
1850
1800
1750
1700
1650
1700
1750
1800
1850
1900
1950
Strain rate

Figure 11

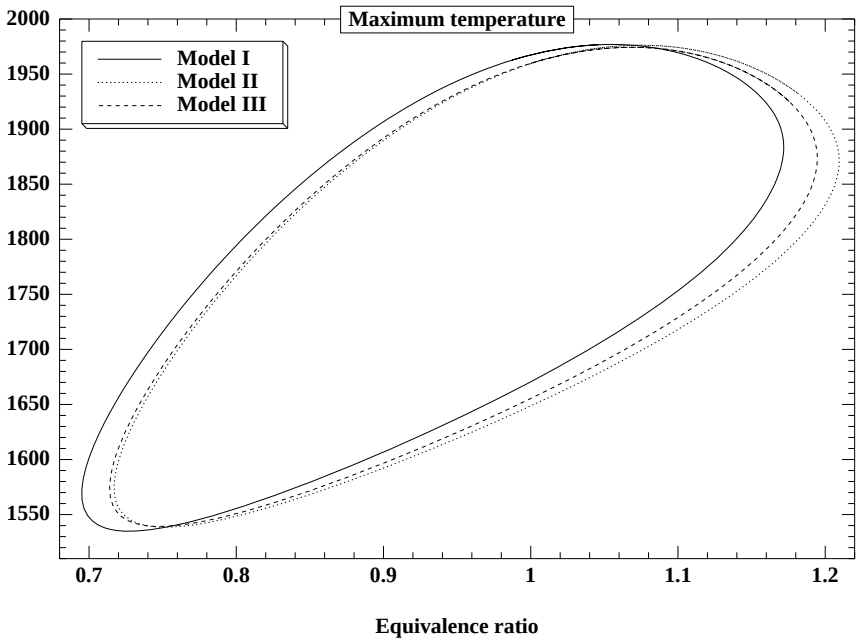
Maximum temperature
Model I
Model II
Model III
2000
1950
1900
1850
1800
1750
1700
1650
1600
1550
0.7
0.8
0.9
1
1.1
1.2
Equivalence ratio

Figure 12